ARTICLE

Check for updates

Neuroligin 2 governs synaptic morphology and function through RACK1-cofilin signaling in *Drosophila*

Yichen Sun [1,2], Moyi Li [1,3✉], Junhua Geng[1], Sibie Meng[1], Renjun Tu[1], Yan Zhuang[1], Mingkuan Sun[4], Menglong Rui[1], Mengzhu Ou[1], Guangling Xing[1], Travis K. Johnson[2,5] & Wei Xie[1,3✉]

Neuroligins are transmembrane cell adhesion proteins well-known for their genetic links to autism spectrum disorders. Neuroligins can function by regulating the actin cytoskeleton, however the factors and mechanisms involved are still largely unknown. Here, using the *Drosophila* neuromuscular junction as a model, we reveal that F-Actin assembly at the *Drosophila* NMJ is controlled through Cofilin signaling mediated by an interaction between DNlg2 and RACK1, factors not previously known to work together. The deletion of DNlg2 displays disrupted RACK1-Cofilin signaling pathway with diminished actin cytoskeleton proteo-stasis at the terminal of the NMJ, aberrant NMJ structure, reduced synaptic transmission, and abnormal locomotion at the third-instar larval stage. Overexpression of wildtype and activated Cofilin in muscles are sufficient to rescue the morphological and physiological defects in *dnlg2* mutants, while inactivated Cofilin is not. Since the DNlg2 paralog DNlg1 is known to regulate F-actin assembly mainly via a specific interaction with WAVE complex, our present work suggests that the orchestration of F-actin by Neuroligins is a diverse and complex process critical for neural connectivity.

[1] School of Life Science and Technology, The Key Laboratory of Developmental Genes and Human Disease, Southeast University, Nanjing 210096, China. [2] School of Biological Sciences, Monash University, Clayton, VIC 3800, Australia. [3] Jiangsu Co-innovation Center of Neuroregeneration, Nantong University, Nantong 226001, China. [4] The Key Laboratory of Modern Toxicology, Ministry of Education, School of Public Health, Nanjing Medical University, Nanjing 211166, China. [5] Department of Biochemistry and Chemistry, and La Trobe Institute for Molecular Science, La Trobe University, Bundoora, VIC 3086, Australia. ✉email: limoyi@seu.edu.cn; wei.xie@seu.edu.cn

Synapses, the sites of communication between neurons and their targets, are in some respects specialized variants of the cell-cell junctions formed by other cell types[1]. The highly specialized neuromuscular junction (NMJ) is one of the well-studied synapses[2]. At these synapses, direct linkage via trans-membrane adhesion molecules plays critical roles in synaptic development, formation, maturation and maintenance[3]. Neuroligins are single-pass transmembrane postsynaptic adhesion molecules involved in synaptic formation and function[4–22]. In recent years, Neuroligins and their binding partners the Neurexins have captured wide attention due to their potent synaptogenic properties and genetic association with autism spectrum disorder (ASD), a developmental neurological disorder[23]. Drosophila has four neuroligin genes (dnlg1–4), which have a close evolutionary relationship to their vertebrate homologs[7]. Due to their multiple, functionally redundant family members, there are still obstacles to directly assessing Neuroligins' effects on synaptic formation. The current data from both mammals and flies strongly support the vital participation of Neuroligins in synaptic function and the maturation of the postsynaptic apparatus[7,14,19,22,24–32]. However, the delicate molecular mechanisms by which Neuroligins regulate these processes are not fully understood.

Previously, using the Drosophila NMJ as a model, we and others showed that all four Drosophila Neuroligins (DNlgs) play roles in synaptic formation and function, including the regulation of bouton growth, subsynaptic reticulum assembly, glutamate receptor (GluR) recruitment, and synaptic transmission[7,14,19,22,27–33]. In a recent study, we found that both DNlg1 and DNlg2 have a positive effect on filamentous actin (F-actin) polymerization, while DNlg1, but not DNlg2, directly interacts with the WAVE regulatory complex (WRC) via its C-terminal interacting sequence to organize postsynaptic F-actin assembly, and thus regulate synaptic structure and function at the NMJ[19]. This suggests that DNlg2 has a positive effect on F-actin polymerization via an unknown WRC-independent pathway.

F-actin polymerization is thought to be mainly mediated by WAVE-Arp2/3 pathway positively and by Cofilin negatively[34–37]. Hence, a potential non WAVE factor candidate is via Cofilin[38], an actin binding protein abundantly expressed at the synaptic level that promotes F-actin depolymerization by both filament severing and monomeric actin (G-actin) dissociation from the pointed ends[38,39]. The depolymerizing function of Cofilin is reported to promote a high rate of actin treadmilling, which occurs when G-actin depolymerized from the pointed ends of the filaments is continuously polymerized onto their barbed ends, allowing continuous and robust actin structural reorganization to take place in dynamic cellular regions including for cytokinesis, axon growth and endocytosis[39–41]. All eukaryotes express at least one member of the essential actin-depolymerizing factor (ADF)/Cofilin family of actin-binding proteins[42]. In Drosophila, the gene twinstar (tsr) encodes the sole Cofilin homolog, which is highly conserved across all eukaryotes, from yeast and plants to mammals[43]. Loss of tsr causes multiple defects in cytokinesis, cell motility, axon growth, planar cell polarity and photoreceptor morphogenesis[42,44]. Loss of Cofilin in the murine nervous system leads to various synaptic and developmental defects and behavioral aberrance[43,45]. Neuronal cytoplasmic rods, which are abnormal hyperactive Cofilin-mediated F-actin aggregates[45], accumulate within neurites, where they occlude neurites and block vesicle transport, and are a likely cause of synaptic loss without neuronal loss[45]. These synaptic dysfunctions may play a role in cognitive dementias and Alzheimer disease[45,46]. In this respect, Cofilin is considered a homeostatic regulator in cell biology[38].

In this study, through immunoprecipitation (IP) and mass spectrometry (MS), we surprisingly uncover a direct interaction between DNlg2 and Receptor for activated C kinase 1 (RACK1, also known as Gnb2l1 in mammals), an evolutionarily conserved scaffolding protein that interacts with multiple signaling molecules concurrently through its seven Trp-Asp 40 (WD40) repeats[47–49]. Based on its wide variety of protein partners, RACK1 has been reported to play a role in diverse processes[47–49]. Germline deletion of RACK1 in Drosophila or mice causes embryonic arrest[48,49]. Beyond these, RACK1 has been reported to be a Cofilin regulator by a genome-wide RNA interference (RNAi) screen in cultured Drosophila S2R+ cells[50]. It is also known to directly interact with Rac1[51,52] and RhoA[53], which are two small GTPases involved in actin skeleton regulation.

Here, we reveal a significant role of DNlg2 in the regulation of the actin cytoskeleton in the postsynaptic NMJ through the RACK1-Cofilin signaling pathway. We find that the dramatic reduction in the amount of F-actin at NMJ in dnlg2 mutants is due to the quantity imbalance between phosphorylated and non-phosphorylated forms of Cofilin. Wildtype and non-phosphorylated forms of Cofilin can reverse NMJ synapse undergrowth and reduce locomotion capability in dnlg2 mutants, while a phospho-mimetic form of Cofilin cannot. The direct interaction between DNlg2 and RACK1 enriches our understanding of the RACK1 function on neuronal system and actin cytoskeleton organization. This study provides insights into the mechanisms by which Neuroligins regulate synaptic formation and function through diverse F-actin regulatory pathways.

Results

Loss of DNlg2 and reduced Cofilin cause similarly dysregulated F-actin assembly and synapse establishment. Previously it was shown DNlg2 has a positive effect on F-actin assembly similar to that of DNlg1[19]. However, the lack of interaction between DNlg2 and the WRC suggested it regulates postsynaptic F-actin assembly via a distinct mechanism to DNlg1. One possibility was that DNlg2 regulates F-actin via the Cofilin pathway because WRC and Cofilin signaling pathways are the two main mechanisms known to regulate F-actin dynamics[34–38]. Additionally, using a low-level ubiquitous driver (da-GAL4), we expressed DNlg2 tagged with EGFP and IP DNlg2-EGFP complexes for MS. The lysates identified several partner proteins of interest, including Cofilin (MS-based data can be found in Data Availability).

To test whether DNlg2 regulates F-actin through Cofilin at the NMJ, we first used an antibody (CF1) raised against Cofilin to examine its localization in wildtype flies. The Drosophila body-wall muscles are innervated by numerous motor neurons that branch over the muscles and form stereotypic NMJ terminal boutons[54]. Our immunostaining revealed Cofilin along the NMJ and the muscle, suggesting that it may have a local function at NMJ (Supplementary Fig. 1a). Next, we asked whether Cofilin influences F-actin distribution at the NMJ. Hence, a Cofilin null mutant, $tsr^{N96A}/+$[55], was used. Consistent with previous studies[19], F-actin was highly enriched at the postsynaptic sites of the wildtype NMJ, displaying a diffuse meshwork-like appearance. In the dnlg2 and cofilin mutant NMJs, however, the amount of F-actin was dramatically reduced (Fig. 1a, b). Since Cofilin promotes the maintenance of the large G-actin pool by providing new actin monomers[56], we also tested the amount of G-actin at the NMJ. In contrast to F-actin and consistent with our expectations, dnlg2 and cofilin mutant NMJs had a significantly increased amount of G-actin compared to WT (Fig. 1c, d). These data suggest that DNlg2 and Cofilin are important for the actin cytoskeleton at the Drosophila NMJ.
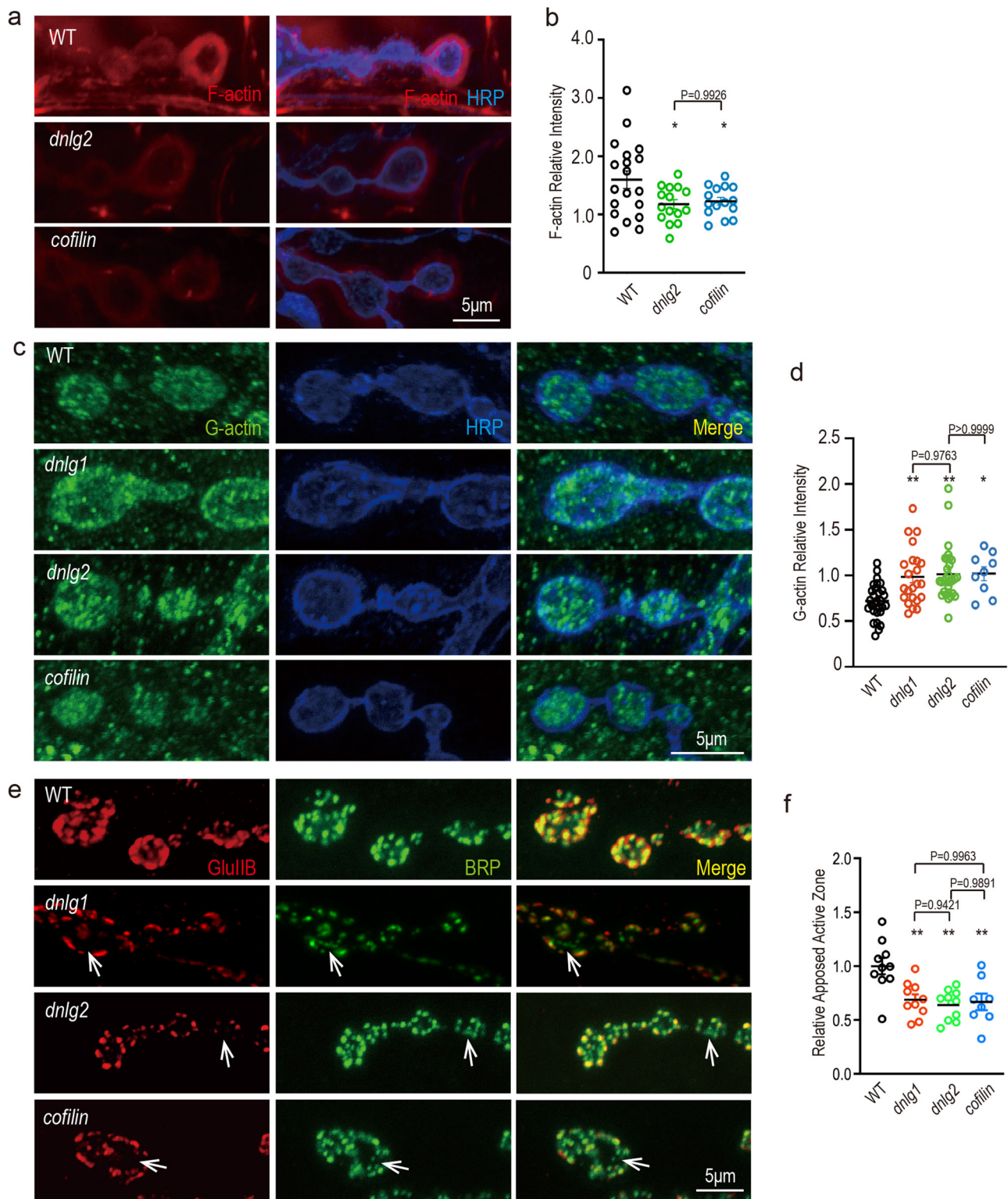
As each bouton contains dozens of glutamatergic synapses[54] and postsynaptic F-actin is important for GluRs recruitment and thus proper synapse establishment[57], we therefore investigated the apposition between postsynaptic GluRs and presynaptic neurotransmitter release sites (active zones). In mutants for DNlg2 and Cofilin, approximately a third of presynaptic active zones were not aligned well with postsynaptic GluRs, while these two markers were mostly apposed in WT (Fig. 1e, f). These results indicate that DNlg2 and Cofilin are necessary for proper NMJ synapse establishment.

DNlg2 regulates postsynaptic F-actin via Cofilin at the NMJ.
Since the *dnlg2* and *cofilin* mutants both showed similar defects in postsynaptic actin organization and GluRs recruitment, we hypothesized that DNlg2 and Cofilin may act together to coordinate NMJ F-actin assembly. Though a previous study showed DNlg1 regulates F-actin through the interaction with WRC, we included *dnlg1* mutants in our tests of the Cofilin pathway. Specifically, we measured the phosphorylated, inactive form of Cofilin, as well as total Cofilin in WT, *dnlg1* and *dnlg2* mutant

Fig. 1 Actin dynamics and pre- and postsynaptic protein apposition are mis-regulated in *dnlg2* mutant NMJs. a F-actin is downregulated in *dnlg2* and *cofilin* mutants. Confocal images of WT (*n* = 19), *dnlg2* mutants (*dnlg2*[KO70/KO70]) (*n* = 15), and *cofilin* mutants (*tsr*[N96A]/+) (*n* = 14) third instar larvae NMJ type Ib boutons at muscles 12/13 labeled with Texas Red phalloidin (red, F-actin) and anti-HRP (blue). **b** Scatter diagram shows a significant decrease in the relative intensity of F-actin in *dnlg2* mutants, and *cofilin* mutants compared with WT. **c** G-actin is upregulated in *dnlg2* and *cofilin* mutants. Confocal images of WT (*n* = 29), *dnlg1* (*dnlg1*[ex1.9/ex2.3]) mutants (*n* = 23), *dnlg2* mutants (*n* = 30), and *cofilin* mutants (*n* = 9) third instar larvae NMJ type Ib boutons at muscles 12/13 labeled with anti-DNase I (green, G-actin) and anti-HRP (blue). **d** Scatter diagram shows a significant increase in the relative intensity of G-actin in *dnlg1* mutants, *dnlg2* mutants, and *cofilin* mutants compared with WT. **e** Relative apposed active zones decrease in *dnlg2* and *cofilin* mutants. Confocal images of WT (*n* = 10), *dnlg1* mutants (*n* = 10), *dnlg2* mutants (*n* = 10) and *cofilin* mutants (*n* = 8), third instar larvae NMJ type Ib boutons at muscle 4 labeled with anti-GluRIIB (red) and anti-nc82 (green, BRP). White arrowheads highlight the zones that GluRIIB cannot correspond to BRP. **f** Scatter diagram shows a significant decrease in the relative apposed active zone in *dnlg1* mutants, *dnlg2* mutants, and *cofilin* mutants compared with WT. Data are presented as mean ± SEM.

adult head and third instar larvae body-wall extracts by immunoblots. Both *dnlg* mutants showed a significant decrease in p-Cofilin level compared to WT (Fig. 2a, b), with no change in total Cofilin (Fig. 2c, d), suggesting that the loss of DNlg1/2 may cause a net increase in Cofilin activity. While we detected a disruption of p-Cofilin in *dnlg1*, hereon we focused our attention on DNlg2. In this regard, these data raise the possibility that DNlg2 promotes postsynaptic F-actin assembly at the NMJ via the modulation of Cofilin.

We reasoned that if DNlg2 acts upstream of Cofilin, then the defects caused by loss of Dnlg2 might be rescued by modulating postsynaptic Cofilin activity. Since Cofilin plays the dual functions to promote F-actin disassembly by severing, and polymerization by supplying actin monomers, we were unsure whether increasing or decreasing Cofilin activity would help actin reorganization and rescue the defects in *dnlg2* mutants[43]. For this reason, we started with overexpression of wildtype (Cofilin[WT]), constitutively active (Cofilin[S3A], which cannot be phosphorylated), and constitutively inactive (Cofilin[S3E], which mimics p-Cofilin[58]) Cofilin with a muscle-specific driver (*C57-GAL4*) under the *dnlg2* mutant background.

In the terms of the declined F-actin level at *dnlg2* mutants NMJ, postsynaptic overexpression of Cofilin[WT] had no significant rescue effect but a restoration trend (Fig. 2e, f). Indeed, both Cofilin[S3A] and Cofilin[S3E] could rescue this deficit, with a stronger rescue effect by Cofilin[S3E] (Fig. 2e, f). However, unlike the wildtype NMJ, in which F-actin organization is evenly spaced and distributed around the bouton (Fig. 2e), F-actin in the *dnlg2* mutants expressing Cofilin[S3E] was organized into snarls and rods, which was visibly abnormal (Fig. 2e). We were therefore curious as to whether other *dnlg2* NMJ deficits could also be rescued.

As a measure of the NMJ growth, bouton number in *dnlg2* mutants was previously found declined[28,59]. While expression of Cofilin[WT] partially increased the bouton number in *dnlg2* mutants, expression of Cofilin[S3A] did so significantly and to a larger degree relative to the *dnlg2* mutant control (Fig. 2g, h). Bouton number in the Cofilin[S3E] rescue line was significantly lower than that of wildtype and comparable to that of *dnlg2* mutants (Fig. 2g, h).

We next looked at synapse establishment in these NMJs and found the aberrant GluRs recruitment in *dnlg2* mutants was strongly restored by expression of wildtype and constitutively active Cofilin (Fig. 3a, b). However, interestingly, Cofilin[S3E] had a much more pronounced rescue effect on the mis-apposition phenotype in *dnlg2* mutants, causing rescue of the phenotype to a level even beyond the wildtype control (Fig. 3a, b). We also noticed orphan boutons[29], a poor synaptic development phenotype, in the *dnlg2* mutants whereby around 10% boutons lost the postsynaptic receptors (Fig. 3c, d). Both Cofilin[WT] and Cofilin[S3A] completely rescued this defect in *dnlg2* mutants, whereas Cofilin[S3E] could not (Fig. 3c, d).

As the stability and integrity of synapses are vital for the maintenance of mature synapse function[60], we further analyzed the synaptic transmission ability and animal behavior of the third-instar larvae. In line with previous studies[28], synaptic transmission capacity was decreased in *dnlg2* mutants, as we detected the declined mEJP amplitude and mEJP frequency (Fig. 4a–c). Postsynaptic expression of Cofilin[WT] and Cofilin[S3A] in the *dnlg2* mutants restored the mEJP amplitude back to levels comparable to those in WT, whereas Cofilin[S3E] did not (Fig. 4a–c). Intriguingly, the mEJP frequency could be rescued by all three Cofilin lines, though Cofilin[S3E] had the weakest rescue effect (Fig. 4a–c), suggesting the Cofilin[S3E] might regulate synaptic transmission via alternative means. In the terms of locomotion, consistent with previous studies[14], *dnlg2* mutants showed severe reduction in crawling ability, covering approximately half the distance of WT (Fig. 4d, e). Postsynaptic expression of Cofilin[WT] and Cofilin[S3A] in the *dnlg2* mutants rescued this defect back to levels comparable to that of WT, whereas Cofilin[S3E] could not (Fig. 4d, e).

Taken together, these results suggest that increasing postsynaptic Cofilin activity buffers the impacts of DNlg2 loss through the maintenance of synaptic morphology and establishment, which in turn preserves normal synaptic transmission capacity and locomotor behavior. As Cofilin function is typically associated with the severing of F-actin rather than its reassembly, these data fit better under a model whereby DNlg2-Cofilin enhances the supply of G-actin monomer required for filament growth.

Additionally, these data also suggest that the NMJ morphological and functional defects observed upon Dnlg2 deficiency are the result of a dysregulation of F-actin assembly, caused by reduced Cofilin activity rather than merely insufficient F-actin levels, as the F-actin stabilization is not sufficient to restore synaptic growth, integrity, transmission, and locomotion.

DNlg2 binds RACK1 and may regulate Cofilin activity via RACK1-mediated Rac1 and RhoA pathways. Having established the relationship between DNlg2 and Cofilin for regulating F-actin assembly at synapse, we next wished understand how DNlg2 signals to Cofilin activity.

To begin, we intended to identify proteins that complex with DNlg2, and may therefore be involved in signaling to Cofilin. In the MS results for DNlg2 IP, a well-known scaffold protein for signaling complexes, RACK1, was detected. To confirm the interactions between DNlg2, Cofilin and RACK1, we enriched DNlg2 complexes from DNlg2-HA-overexpressing (*da-GAL4*) *Drosophila* adult head extracts and performed co-IP analysis (Fig. 5a). Both RACK1 and Cofilin were detected (Fig. 5a). Similarly, DNlg2 and RACK1 were detected in the IP lysates from Cofilin-GFP-overexpressing (*da-GAL4*) *Drosophila* adult head tissue (Fig. 5b). We also validated the interaction between Nlg1 and RACK1 in mouse brain (Supplementary Fig. 2a). Mouse Nlg1
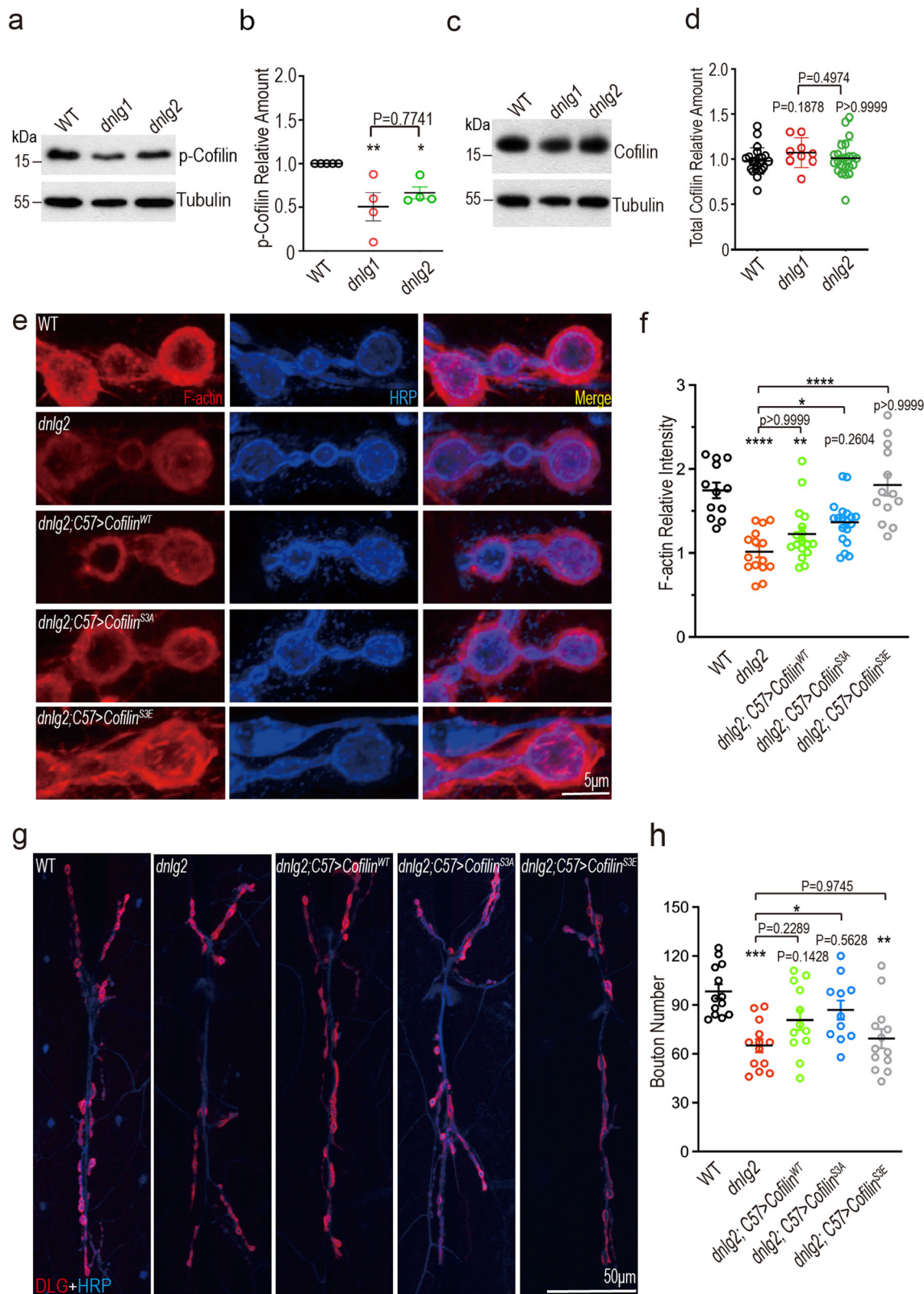
is the homolog of DNlg2 in *Drosophila* suggesting that the interaction between Nlgs and RACK1 is conserved through to mammals. These results strongly suggest that DNlg2 exists in complex with both RACK1 and Cofilin in vivo.

To further determine which part of DNlg2 binds RACK1 and Cofilin, we performed an additional MS on the extracellular and intracellular domains of DNlg2, respectively (MS-based data can

be found in Data Availability). RACK1 was identified as an interactor of the DNlg2 intracellular domain, but not the extracellular domain (Table 1). Cofilin, however, was associated with both domains (Table 1). We also synthesized N- and C-terminal fragments of DNlg2 bound to the Strep tag II, respectively (Fig. 5c), and performed in vitro pull-down assays with synthesized *Drosophila* RACK1. Consistent with the MS

Fig. 2 The decreased F-actin level and bouton number at the NMJ of *dnlg2* mutants could be rescued by modulating postsynaptic Cofilin activity.
a p-Cofilin is downregulated in *dnlg2* mutants. Muscle lysates of the third instar larvae from WT ($n = 5$), *dnlg1* mutants ($n = 4$), and *dnlg2* mutants ($n = 4$) were subjected to western blots with anti-p-Cofilin antibody. **b** Scatter diagram shows the relative amount of p-Cofilin in both lines in **a**. p-Cofilin expression was dramatically inhibited in *dnlg1* mutant and *dnlg2* mutant. **c** Muscle lysates of the third instar larvae from WT ($n = 23$), *dnlg1* mutants ($n = 9$), and *dnlg2* mutants ($n = 23$) were subjected to western blots with anti-Cofilin antibody. **d** Scatter diagram of the total Cofilin relative amount in **c**. There was no change in the total Cofilin expression in *dnlg1* mutants and *dnlg2* mutants. **e** Confocal images of the third instar larvae NMJs from WT ($n = 12$), *dnlg2* mutants ($n = 15$), *dnlg2; C57 > Cofilin*^{WT} ($n = 17$), *dnlg2; C57 > Cofilin*^{S3A} ($n = 19$) and *dnlg2; C57 > Cofilin*^{S3E} ($n = 13$). Type Ib boutons at muscles 12/13 were labeled with Texas Red phalloidin (red) and anti-HRP (blue). **f** Quantitative data of **e** shows the decreased F-actin relative intensity in *dnlg2* mutants and restoration by muscle expression of Cofilin. **g** Confocal images of the third instar larvae NMJs from WT ($n = 13$), *dnlg2* mutants ($n = 13$), *dnlg2; C57 > Cofilin*^{WT} ($n = 12$), *dnlg2; C57 > Cofilin*^{S3A} ($n = 11$) and *dnlg2; C57 > Cofilin*^{S3E} ($n = 13$). Type Ib boutons at muscles 6/7 were labeled with anti-DLG (red) and anti-HRP (blue). **h** Quantitative data of **g** shows the reduced bouton number in *dnlg2* mutants and restoration by muscle expression of Cofilin. Data are presented as mean ± SEM.

results, only the C-terminal of DNlg2 was found to bind RACK1 (Fig. 5d). These combined results suggest the specific direct interaction between DNlg2 C-terminal fragment and RACK1, and provide a basis for the direct regulation of F-actin regulation to influence synapse morphology and function.

As RACK1 has been linked to Cofilin phosphorylation previously[50,53], we were curious to know whether the expression or localization of RACK1 is abnormal when DNlg2 is deficient, which in turn may affect Cofilin. Although no changes in the expression level of RACK1 were detected in *dnlg2* mutants and the striatum of Nlg1 knockout mice (Supplementary Fig. 2b–e), we found that RACK1 showed a diffused distribution at the NMJ of *dnlg2* mutants (Fig. 5k), suggesting a role of DNlg2 in regulating the localization of RACK1, which may further affect its function. We also detected an increase in total Cofilin levels when ubiquitously knocked down RACK1 by *da-Gal4* (Supplementary Fig. 2b–e).

Under the canonical model of Cofilin regulation, the G-protein Rac1 activates PAK1, a serine/threonine kinase that phosphorylates LIMK, which in turn phosphorylates Cofilin[58]. There is also an alternative pathway whereby LIMK is activated by RhoA-ROCK[58]. To see whether one or both of these pathways are working in DNlg2-Cofilin signaling, we looked at the activity of Rac1 and RhoA in *dnlg2* mutants using antibodies that detect GTP-bound (active) and their total protein level, respectively. We detected strong reduction in both activated Rac1 and RhoA in *dnlg2* mutants (Fig. 5e–h), which is consistent with the reduction of p-Cofilin detected in *dnlg2* mutants, suggesting DNlg2 may regulate the activity of Cofilin through Rac1 and RhoA.

Previous studies have identified RACK1 as an interactor of Rac1 in rice[51], *C. elegans*[52], and mouse[61]. We therefore hypothesized that RACK1 might similarly directly interact with Rac1 in *Drosophila*. To test this, we co-expressed GFP-tagged *Drosophila* RACK1 and mcherry-tagged *Drosophila* Rac1 in 293T cells and performed co-IP. We detected Rac1-mcherry only when co-expressing RACK1-GFP (Fig. 5i), suggesting that these proteins form a complex in vitro. Next, we enriched autologous active Rac1 in 293T cells and detected RACK1 in Rac1-GTP pull-down lysates (Fig. 5j). This validated the interaction between active Rac1 with RACK1 from 293T cells. According to bioinformatic analysis, the Rac1 and RACK1 protein sequences between *Drosophila* and human are highly similar (Supplementary Fig. 2h), and these two proteins have a high potential to form a complex in fly, as well as human and mouse (Supplementary Fig. 2i). Additionally, the expression level of activated Rac1 was reduced when knocking down RACK1 (Fig.5m, n), in line with our observations from *dnlg2* mutants, suggesting that the interaction between RACK1 and Rac1 is important for the activity of Rac1, and may further regulate Cofilin activation. Taken together these results support a model for DNlg2 regulation of Cofilin via DNlg2-RACK1-RhoA and DNlg2-RACK1-Rac1 pathways (Fig. 6).

Discussion

Neuroligins affect synaptic development and functions largely through regulating F-actin assembly. Previously, we found DNlg1 can directly interact with WRC to promote F-actin polymerization through WRC-Arp2/3 signaling[19]. We observed similar F-actin downregulation in *dnlg2* mutants but it remained unknown how DNlg2 regulated F-actin organization, as DNlg2 does not bind directly with WRC. In this study, we detected p-Cofilin downregulation and G-actin promotion in *dnlg2* mutants, which suggests that the depolarization of F-actin is accelerated in *dnlg2* mutants. Then we observed most of F-actin related NMJ defects can be rescued by wildtype and activated forms of Cofilin. Activated Rac1 and RhoA, the positive regulators of Cofilin phosphorylation are dramatically downregulated in *dnlg2* mutants at the same time, thus, suggesting the Cofilin phosphorylation pathway is disrupted. The reduced Rac1 and RhoA activation in *dnlg2* mutants is likely to cause a major imbalance between activated and inactivated Cofilin, ultimately resulting in accelerated F-actin depolymerization.

How can DNlg2 suppress Rac1 and RhoA activation and further suppress Cofilin phosphorylation? Our MS and co-IP experiments fished out an actin related regulator, RACK1 in the complex with DNlg2, and the further MS analysis indicates that RACK1 specifically interacts with DNlg2 intracellular domain instead of extracellular domain, whereas Cofilin does not display this unique feature. These finding highly suggest that the C-terminal of DNlg2 can directly interact with RACK1 to connect DNlg2 and small G-proteins regulating Cofilin activity, as shown in Fig. 6.

RACK1 has gained recent attention in neuroscience due to its rediscovered potential functions in neural systems[62]. It is reported to be involved in axon growth and guidance in *C. elegans*[52]. Additionally, it can act as the regulator of the actin cytoskeleton in migrating cells and growth cones[63,64]. More recent studies found its role in mouse cerebellar and cortex development through regulating multiple different pathways in neural stem cells[65,66]. Our observation that knocking down RACK1 reduced active Rac1 might be a hint of how RACK1 functions, because Rac1 appears to regulate a diverse array of cellular events[58,67–70]. We also found a conserved interaction between Nlg1 and RACK1 in mouse brain tissue, and it would be interesting to test whether Nlg1 functions through RACK1 in mammalian neural system.

An unexpected finding was that DNlg2 deletion had no discernible effect on RACK1 accumulation, or total Rac1 and RhoA in cells. It seems that DNlg2 deletion only affects the distribution of RACK1, destabilizing RACK1-Rac1-Cofillin or RACK1-RhoA-Cofillin complexes, and therefore affecting Rac1 or RhoA activation. Surprisingly, although most *dnlg2* defects could only be restored by Cofilin^{WT} and Cofilin^{S3A}, Cofilin^{S3E} rescued F-actin, apposed active zones, and the mEJP frequency in *dnlg2* mutants. These restoration effects might due to the remaining F-actin
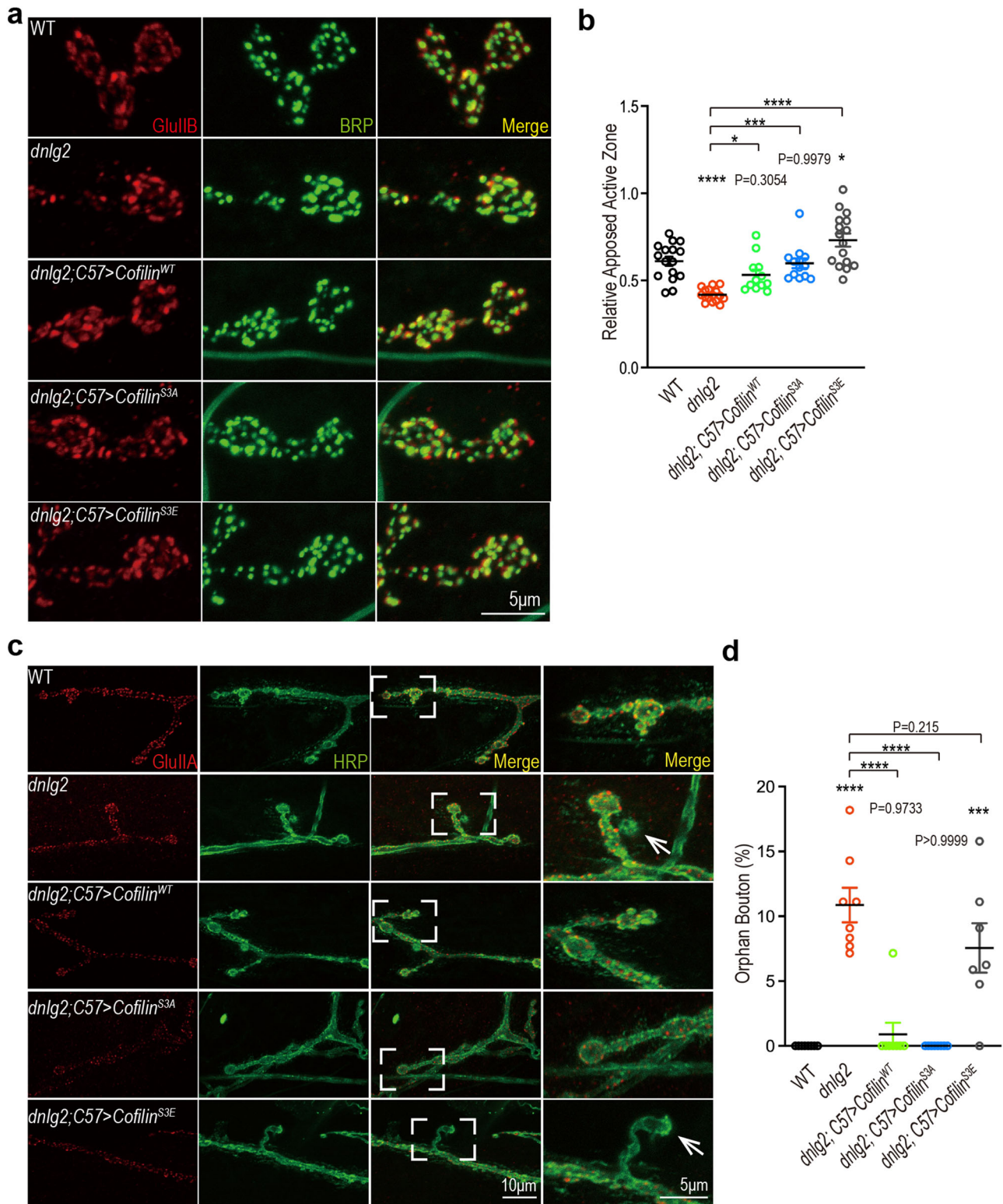
Fig. 3 The aberrant GluRs recruitment at the NMJ of *dnlg2* mutants could be rescued by modulating postsynaptic Cofilin activity. a Confocal images of the third instar larvae NMJs from WT ($n = 16$), *dnlg2* mutants ($n = 16$), *dnlg2; C57 > Cofilin*^{WT} ($n = 12$), *dnlg2; C57 > Cofilin*^{S3A} ($n = 13$) and *dnlg2; C57 > Cofilin*^{S3E} ($n = 16$). Type Ib boutons at muscle 4 were labeled with anti-GluRIIB (red) and anti-nc82 (green, BRP). **b** Quantitative data of **a** shows the decreased apposed active zone in *dnlg2* mutants and restoration by muscle expression of Cofilin^{WT}, and Cofilin^{S3A}. Cofilin^{S3E} over-rescued this defect. **c** Confocal images of the third instar larvae NMJs from WT ($n = 8$), *dnlg2* mutants ($n = 8$), *dnlg2; C57 > Cofilin*^{WT} ($n = 8$), *dnlg2; C57 > Cofilin*^{S3A} ($n = 8$) and *dnlg2; C57 > Cofilin*^{S3E} ($n = 7$). Type Ib boutons at muscle 4 were labeled with anti-8B4D2 (red, GluRIIA) and anti-HRP (blue). The right lane shows the amplified contents framed in merge images. White arrowheads highlight the orphan boutons. **d** Quantitative data of **c** shows the increased percentage of orphan bouton in *dnlg2* mutants and restoration by muscle expression of Cofilin^{WT} and Cofilin^{S3A}. Data are presented as mean ± SEM.
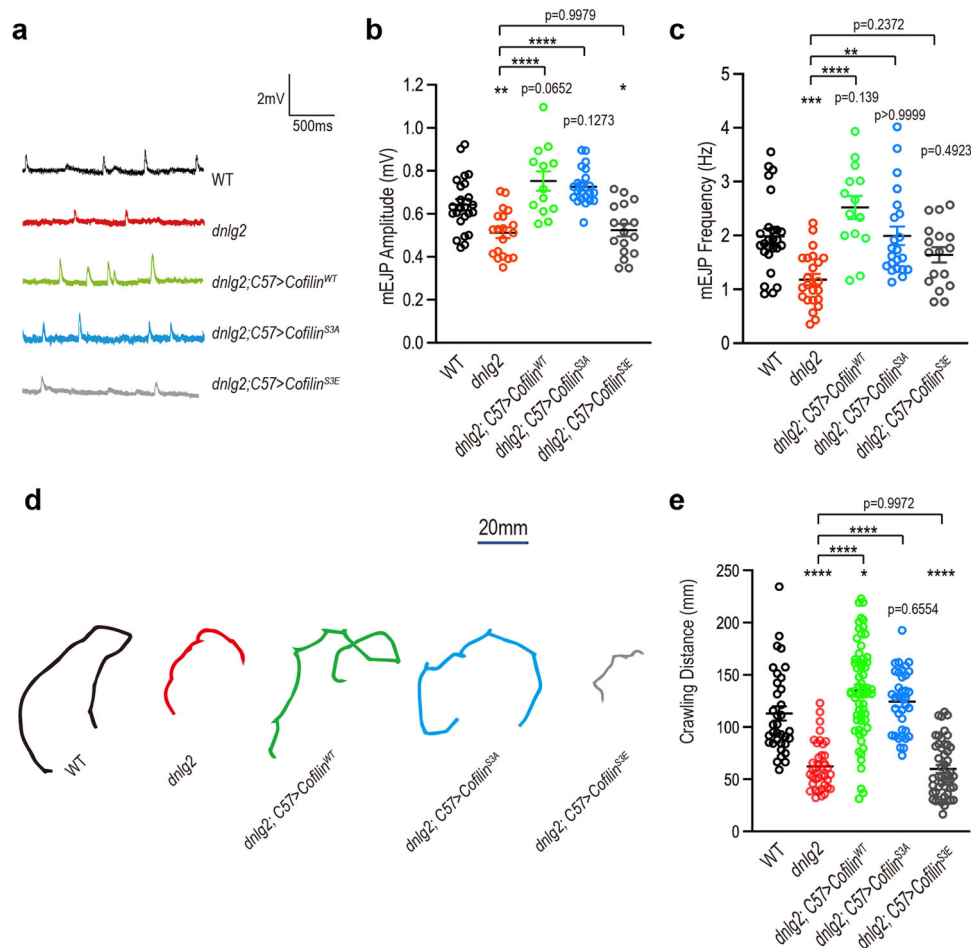
Fig. 4 The aberrant synaptic transmission and locomotion activity in *dnlg2* mutants could be rescued by modulating postsynaptic Cofilin activity.
a Representative trace of the mEJP. **b** Scatter diagram of the mean mEJP amplitude (in mV) from WT ($n = 24$), *dnlg2* mutants ($n = 19$), *dnlg2;*
C57 > Cofilin[WT] ($n = 13$), *dnlg2; C57 > Cofilin*[S3A] ($n = 22$) and *dnlg2; C57 > Cofilin*[S3E] ($n = 17$) third instar larvae. **c** Scatter diagram of the mean mEJP
frequency (in Hz) from WT ($n = 26$), *dnlg2* mutants ($n = 23$), *dnlg2; C57 > Cofilin*[WT] ($n = 14$), *dnlg2; C57 > Cofilin*[S3A] ($n = 22$) and *dnlg2; C57 > Cofilin*[S3E]
($n = 17$) third instar larvae. **d** Representative traces of a 3-min crawling of WT (total $n = 35$), *dnlg2* mutants ($n = 37$), *dnlg2; C57 > Cofilin*[WT] ($n = 63$), *dnlg2;*
C57 > Cofilin[S3A] ($n = 37$) and *dnlg2; C57 > Cofilin*[S3E] ($n = 49$) third instar larvae. **e** Quantification of a 3-min crawling distance (in mm) in **d**, showing a
reduced locomotor activity in *dnlg2* mutants and restoration by muscle expression of Cofilin[WT] and Cofilin[S3A]. Data are presented as mean ± SEM.

depolymerizing activity in Cofilin[S3E], which is about 10% of the
wildtype Cofilin[71]. However, it is still puzzling why Cofilin[S3E] had
a stronger rescue effect than Cofilin[WT] and Cofilin[S3A] on F-actin
or apposed active zone rescue experiments. These suggest the
transition between activated and inactivated Cofilin is more
complicated than our expectation, and thus requires further
investigation.

The *dnlg1* mutant also displayed disrupted p-Cofilin accumu-
lation. This result is in contrast with our original hypothesis that
DNlg1 and DNlg2 may have distinct F-actin regulation pathways.
F-actin organization is rescued by recovering the interaction of
DNlg1 and WRC[10] in *dnlg1* mutants, so it remains to be known
how the observed p-Cofilin down-regulation contributes to *dnlg1*
phenotypes. One possibility is that DNlg1 regulates F-actin
assembly primarily via the WAVE complex but also utilizes
Cofilin. It would be interesting see if Cofilin[WT], Cofilin[S3A] or
Cofilin[S3E] can partially reverse *dnlg1* phenotypes.

There are two main limitations to this study. First, despite we
detected the disorganized F-actin like snarls and rods in the *dnlg2*
mutants expressing Cofilin[S3E] by confocal, a higher resolution
imaging modality might be able to better resolve the disorganized
F-actin, and to investigate the difference compared to the evenly
spaced and distributed F-actin organization. Second, we showed

that RACK1 can directly interact with and regulate Rac1 activity.
While we would like to confirm this via other approaches,
unfortunately, there is a lack of effective immunofluorescence
staining antibodies to detect the in vivo Rac1. Development of
such reagents would enable the localization of Rac1 in RACK1
knockout or RNAi *Drosophila* lines.

Taken together, we discover a previously unknown DNlg2-
RACK1-Cofilin signaling pathway to suppress the F-actin depo-
lymerization process. This is different to how DNlg1 primarily
regulates synaptic morphology and function through WRC in
Drosophila NMJ. These diverse F-actin assembly regulatory
mechanisms of Neuroligins at the *Drosophila* NMJ suggests the
potential for similar mechanisms present in other higher animals
and even in humans. These findings provide unique insights to
further understand the basic working principles behind normal
neural functions and molecular pathogenesis of neural disorders
like ASD.

Methods
Fly stocks. All flies were reared at 25 °C in standard medium. The
w^{1118} flies were used as WT controls in this study. The following
fly mutants were used: *dnlg1* mutant: *dnlg1*[ex1.9/ex2.3], a
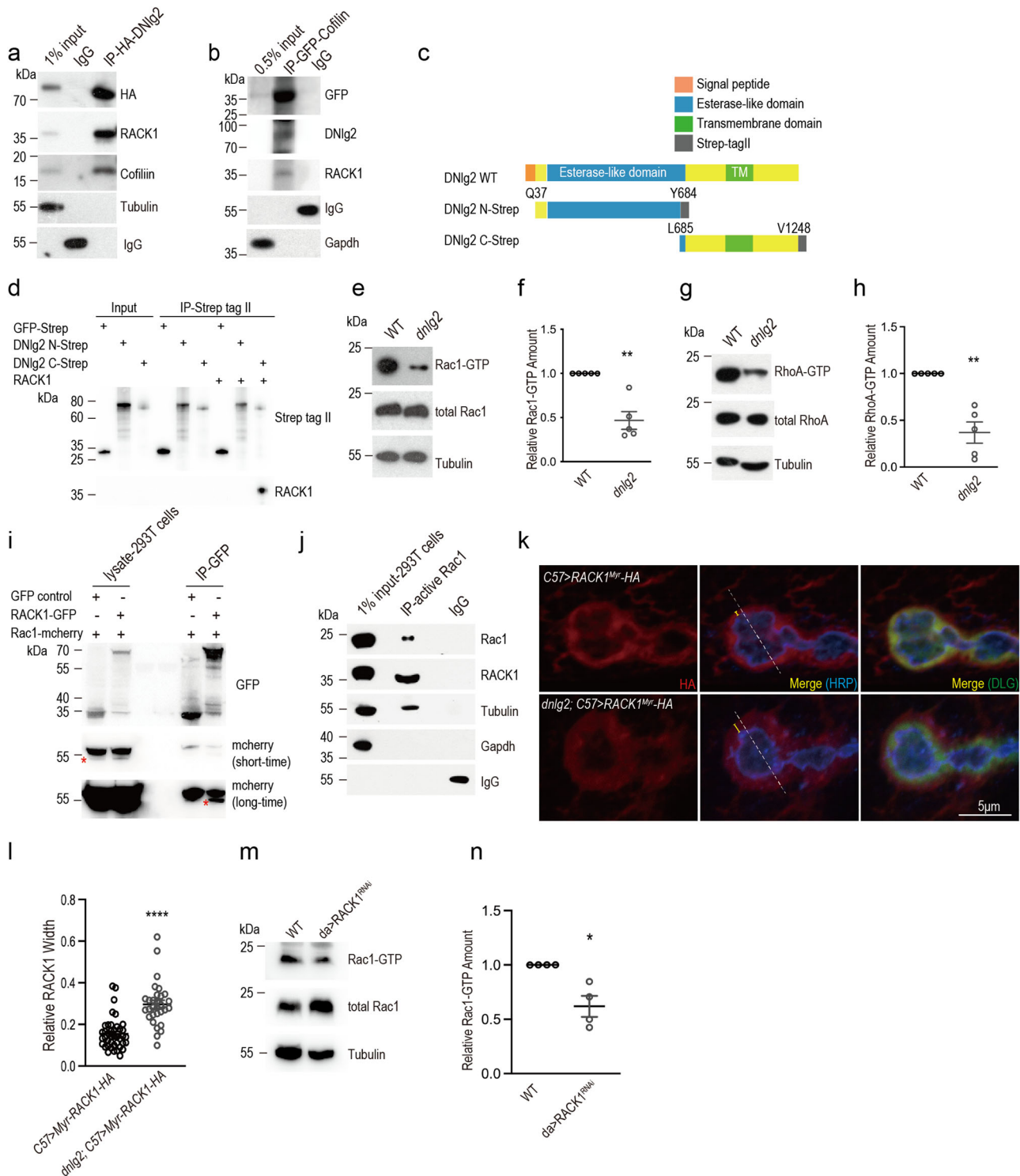
heterozygous mutant combined with two excision alleles[7]; *dnlg2* mutant: *dnlg2^KO70^* generated by our lab, which lost the first exon as well as the expression of DNlg2[14]; *cofilin* mutant: *tsr^N96A^/+* (BDSC, 9108). *tsr^N96A^* is a null allele, which has a 676 bp deletion in the 5′ region including the first exon, consistent with a functional loss of Cofilin[55]. As its homozygous mutant is lethal before the end of first instar larval stage, heterozygous mutant was used here. *rack1* mutant: *rack1^EY00128/1.8^*, a heterozygous mutant combined with two null alleles (BDSC, 15000 and 24152); RACK1^RNAi^ (VDRC, V27858). *UAS-Myr-RACK1-HA* is a membrane-tethered form of RACK1 by adding a myristoylation

signal at its N-terminus[72]. The muscle-specific driver *C57-Gal4* and systemic driver *da-Gal4* were obtained from BDSC.

Three muscle-specific rescue lines were crossed as:
dnlg2^KO70^; C57-GAL4 > UAS-Cofilin^WT^-EGFP
dnlg2^KO70^; C57-GAL4 > UAS-Cofilin^S3A^-EGFP
dnlg2^KO70^; C57-GAL4 > UAS-Cofilin^S3E^-EGFP
We generated *UAS-Cofilin-EGFP* by inserting the full-length Cofilin protein coding sequence into pUAST-EGFP-attB vector, then Xia Yao (Qing Zhang lab, Model Animal Research Center of Nanjing University) helped to injected the resulting plasmids into embryos of attP transgenic flies (BDSC, 35568). Transgenic fly

Fig. 5 DNlg2 can interact with RACK1 and Cofilin, and RACK1 can potentially interact with active Rac1. a DNlg2, RACK1 and Cofilin can interact with each other in vivo. IP lysates was enriched from *da-GAL4 > UAS-DNlg2-HA* adult brain extracts with anti-HA antibody. **b** DNlg2, RACK1 and Cofilin can interact with each other in vivo. IP lysates was enriched from *da-GAL4 > UAS-Cofilin-GFP* adult brain extracts with anti-GFP antibody. **c** Schematic diagram of the synthesis N-terminal (Q37-Y684) and C-terminal (L685-V1248) fragments of DNlg2 bound to the Strep tag II. **d** DNlg2 binds RACK1 through its C-terminal fragment. Only the C-terminal of DNlg2 can directly bind to RACK1, whereas DNlg2 N-terminal cannot. **e** Western blots show the level of Rac1-GTP in adult heads of WT and *dnlg2* mutants. **f** Scatter diagram of the Rac1-GTP relative amount in **e**, indicating the decreased Rac1-GTP in *dnlg2* mutants. **g** Western blots show the level of RhoA-GTP and total RhoA in adult heads of WT and *dnlg2* mutants. **h** Scatter diagram of the RhoA-GTP relative amount in **g**, indicating the decreased RhoA-GTP in *dnlg2* mutants. **i** IP from HEK293T extracts with overexpression of *Drosophila* RACK1-GFP and Rac1-mcherry, enriched with GFP antibody. The result suggests *Drosophila* RACK1 physically interacts with *Drosophila* Rac1 in vitro. The asterisks indicate the proper bands. **j** Active Rac1 can interact with RACK1 in HEK293T cells. HEK293T cell lysates were subjected to a pull-down assay with GST-PAK-PBD agarose beads. **k** Confocal images of the third instar larvae NMJs from *C57>Myr-RACK1-HA* ($n = 41$) and *dnlg2; C57>Myr-RACK1-HA* ($n = 30$). Type Ib boutons at muscle 4 were labeled with anti-HA (red, tagged with RACK1[Myr]), anti-HRP (blue) and anti-DLG (green). **l** Quantitative data of **k** shows the relative RACK1 width on boutons. **m** Western blots show the level of Rac1-GTP in the third instar larvae NMJs from WT ($n = 4$) and *da > RACK1[RNAi]* ($n = 4$). **n** Scatter diagram of the Rac1-GTP relative amount in *n*, indicating the decreased Rac1-GTP when knocking down RACK1. Data are presented as mean ± SEM.

Table 1 Mass spectrometry analysis for the extra- and intracellular domains of DNlg2 GST pull down lysates from *Drosophila* adult heads.

MS detected protein	DNlg2		RACK1		Cofilin	
GST tagged domain	DNlg2-E	DNlg2-I	DNlg2-E	DNlg2-I	DNlg2-E	DNlg2-I
Pep Count[a]	211	0	0	6	20	17
Unique Pep Count[b]	18	0	0	6	5	9
Cover Percent[c]	18.67%	0	0	19.18%	39.19%	67.57%

E = extracellular domain (M1-S965).
I = intracellular domain (A989-V1248).
[a]The number of total detected peptide reads for a protein acquired in MS analysis.
[b]The number of unique peptides acquired from MS analysis.
[c]Coverage of peptide reads over the whole protein sequence.

strains were generated based on the φ31-mediated integration system using the landing site at the cytological position 87B[73]. The transgenes were subsequently crossed into a *w1118* background. For *UAS-Cofilin[S3A]-EGFP* and *UAS-Cofilin[S3E]-EGFP* strains, we changed two or three bases so the Serine3 at the phosphorylation site can be changed to Alanine or Glutamic residue.

cDNA PCR with the following primers were performed to generate the recombinant plasmids.

cofilin-F: 5'-tgaatagggaattgggaattcATGGCTTCTGGTGTAACTGTGTCTG-3';

cofilinS3A-F: 5'-tgaatagggaattgggaattcATGGCTGCGGGTGTAACTGTGTCTG-3';

cofilinS3E-F: 5'-tgaatagggaattgggaattcATGGCTGAGGGTGTAACTGTGTCTG-3';

cofilin-R: 5'-gatctgcgcgttaacgaattcTTATTGGCGGTCGGTGGC-3'.

These transgenic strains were verified by PCR and Immunochemistry analysis:

verify-F: 5'-GTAACCAGCAACCAAGTAAATC-3';

verify-R: 5'-TAAATCTCTGTAGGTAGTTTGTCC-3'.

Mice. C57BL/6 mice were used as wildtype mice, purchased from Huangchuang Sino. Nlg1[KO] mice were generated previously[74]. The mice were housed under standard laboratory conditions with access to food and water ad libitum, stable temperature (22 ± 1 °C), and 12-h light–dark cycle (lights on at 07:00). All animal care and experimental procedures were followed by the Animal Experimental Ethical Guide of Southeast University and Animal Core Facility of Nanjing Medical University.

The striatum tissues from 3-4 week-old mice (two males and two females) were used for the western blot experiments detecting the RACK1 contents. The cortex and hippocampus tissues from 3-4 week-old male C57BL/6 mice were used for the co-IP experiments.

Larval locomotion activity detection. To monitor larval locomotion, transparent dishes (diameter, 8.5 cm) with 3.5% agar substrate were used as an arena for crawling larvae. Grape purple food colorant was added until the substrate presented a dark purple color. In each trial, a single wandering third-instar larvae was transported to the center of the arena. The movement of larvae was visualized via a standard commercial video camera (resolution, 640×480) for 3 min. Tracker software was written in Python to track the trajectory, and 3-min trajectory distances were calculated by AIM-LSM for assessing larval locomotion activity.

Western blot analysis. In brief, adult fruit fly heads or third-instar larvae body-wall muscle were homogenized with $2 \times$ SDS loading buffer (Takara, H621), and the total protein lysates were separated by precast protein gel (GenScript, Sure PAGE, M00653) and electro-transferred onto polyvinylidene difluoride membranes. Immobilized proteins on the membrane were probed with proper primary antibodies at shaker in 4 °C overnight. The samples were then incubated with HRP-conjugated secondary antibodies at room temperature for 2 h. The targeted proteins were visualized with high-sig ECL western blotting substrate from Tanon and SuperSignal West Femto Maximum Sensitivity substrate from Thermo Scientific. The blots shown are representative of ≥3 independent experiments. The antibodies used in this study can be found in Supplementary Data. 1.

Immunoprecipitation. Briefly, adult heads were homogenized and lysed in ice-cold cell lysis buffer for Western and IP (Beyotime, P0013J) added EDTA-free Protease Inhibitor Cocktail (Roche). The lysates were kept on shaker at 4 °C for 60 min and centrifuged at 12,000 rpm at 4 °C for 15 min, twice. The supernatant was incubated with proper antibody on shaker at 4 °C overnight, and incubated with Pierce Protein A/G Agarose (Thermo Scientific) at room temperature for 60 min in the second
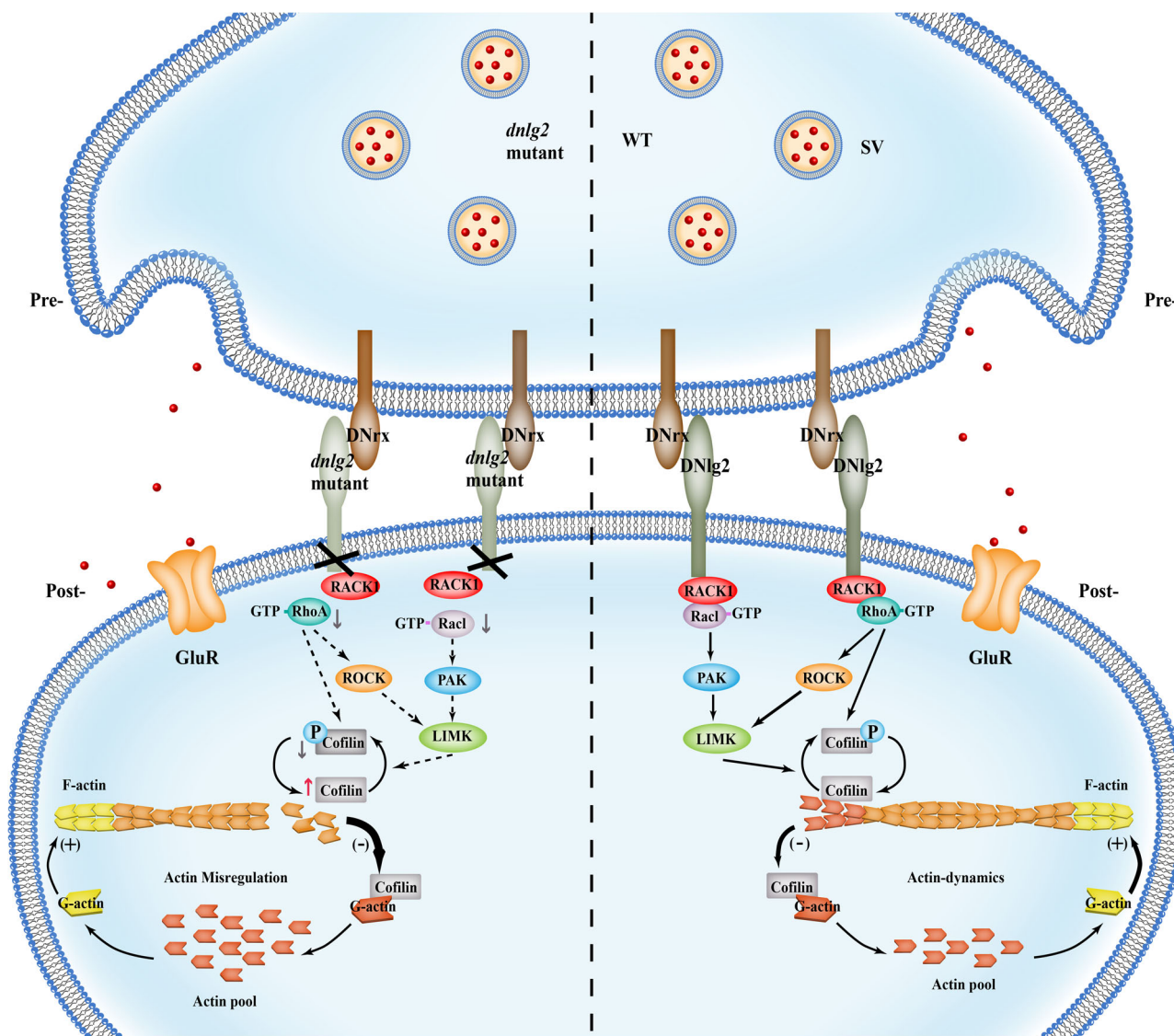
Fig. 6 Model for Neuroligin2-RACK1-Cofilin signaling in WT and *dnlg2* mutants. In WT *Drosophila* NMJs, postsynaptic DNlg2 interacts with RACK1 which can form a complex with downstream Rac1-Cofilin or RhoA-Cofilin signaling components to activate Cofilin phosphorylation. Only if phosphorylated and non-phosphorylated Cofilin kept in a right balance, can actin polymerization/depolymerization be maintained in a good balance. Otherwise, disruption of DNlg2 will destabilize the big DNlg2-RACK1-Rac1 (or RhoA)-Cofilin-signaling complex. This disruption will affect Rac1 and RhoA activation and therefore inhibit downstream Cofilin phosphorylation. The downregulated p-Cofilin will break F-actin polymerization/depolymerization balance to accelerate its depolymerization.

day. Then the lysates were centrifuged at 2000 rpm at 4 °C for 2 min and discard the supernatant. The Agarose was subsequently washed three times with lysis buffer, and proteins were eluted by boiling the beads in 2 × SDS loading buffer. Following, centrifuged at 12,000 rpm at room temperature for 2 min and the supernatant was used for western blot analysis.

For in vitro immunoprecipitation, N-terminal (extracellular part containing the esterase-like domain, residues Q37-Y684) and C-terminal (transmembrane and intracellular domains, residues L685-V1248) fragments of DNlg2 were synthesized bound to the Strep tag II, respectively. GFP-Strep tag II was used as the negative control. Proteins were enriched by MagStrep beads (iba, 2-4090-002). Input and bound fractions were analyzed by immunoblotting. The antibodies used in this study can be found in Supplementary Data. 1.

NMJ staining and image analysis. In brief, the body-wall muscles from third instar larvae were dissected in PBS solution and fixed them for 40 min with 4% paraformaldehyde or for 5 min with chilled methanol. Then, the fixed samples were washed four times in 0.3% PBST (0.3% Triton X-100 in PBS), blocked in blocking solution (0.5% BSA in 0.3% PBST) for 1 h, and incubated with primary antibody at 4 °C overnight. Secondary antibodies were incubated at room temperature for 2 h. Then the samples were washed extensively and mounted in VectaShield mounting medium (Vector Laboratories). All images were collected using an LSM 710 Confocal Station (Zeiss) and analyzed by Image J software. The antibodies used in this study can be found in Supplementary Data. 1.

For measurements of fluorescence intensity, we set an arbitrary threshold for each channel based on the difference in intensity between the NMJ and the background regions. The sum of the pixels with intensities above the threshold was recorded by ImageJ. For comparison of fluorescence intensities between genotypes, all samples were processed simultaneously and under identical conditions. Anti-HRP staining signal was used as a control signal.

For F-actin staining, NMJ samples were incubated with a high concentration of Texas Red-conjugated phalloidin (1:6) for 13 min at room temperature after secondary antibodies incubation and cleaning. Images were collected at muscles 12/13, because the distance between the boutons and the myofibril in that muscle is relatively large, thus reducing the interference from a strong F-actin-stained background due to myofibril[75]. We performed statistical analyses as described in the source data tables.

Quantification of active zones was performed using a previous modified method[7]. The apposed active zones were defined as active zones correspond to GluRs. We co-applied GluRIIB rabbit polyclonal antibody and BRP mouse monoclonal antibody (nc82) for immunofluorescence staining. A branch of bouton clusters (usually 8–10 boutons) from muscle 4 of segment A3 were included in the analysis instead of quantifying only terminal boutons. To avoid subjective variation in the counting the numbers of non-overlapping BRP/GluRIIB spots, the ratio of overlapping BRP area to the total BRP area, namely percentage apposed AZ area was used to represent the extent of apposition. That method is very similar to the way that the extent of co-localization of presynaptic and postsynaptic proteins in mammalian systems is quantified[76]. The BRP spots in single-channel images and the overlapping spots of BRP and GluRIIB in corresponding two-channel merged images were respectively detected using ImageJ. Then, the total area of the BRP spots and that of the BRP/GluRIIB overlapping spots were quantified using the 'analyze particles' function in ImageJ. We defined the relative apposed active zone as the ratio of the total BRP/GluRIIB overlapping spot area to the total BRP spot area.

Rac1 activity assay. The heads of approximately 500 adult flies or the body wall muscle of approximately 300 third instar larvae were homogenized and lysed to gain sample. For detecting the relative levels of active Rac1, Pak-PBD pull-down assay (Thermo Scientific, 16118) was used. The anti-Rac1 monoclonal antibody (1:1000 dilution) was used to detect total and active Rac1 levels. The Rac1-GTP relative amount is calculated by dividing Rac1-GTP by tubulin.

Rho activity assay. The heads of approximately 500 adult flies were homogenized and lysed to gain sample. For detecting the relative levels of active Rho, Rhotekin-RBD pull-down assay (Thermo Scientific, 16116) was used. The anti-Rho monoclonal antibody (1:1000 dilution) was used to detect total and active Rho levels. The Rho-GTP relative amount is calculated by dividing Rho-GTP by tubulin.

Electrophysiology. Third instar larvae were dissected and intracellular membrane potentials were recorded as previously described[14]. Briefly, wandering third instar larvae were dissected in Ca^{2+}-free HL3.1 saline, fat and gut in the body were removed, brain and VNC were cut, and the body wall was carefully spread out to expose muscle for avoiding damage the muscle architecture. Then HL3.1 saline was used to wash and immerser the sample. We chose muscle 6 in the A3 segment for recording using the recording electrodes (20–50 MΩ) filled with 3 M KCl. Miniature EJPs (mEJPs) were recorded for a period of 60 s. All recordings were conducted at room temperature with an Axoclamp 900 A amplifier (Molecular Devices, Sunnyvale, CA) in bridge mode. The data were digitized with a Digitizer 1322 A (Molecular Devices). We used Clampfit 10.2 to analyze the data. Only the recordings with resting membrane potentials ranging from −60 to −65 mV were used for analysis.

All recordings were conducted in modified HL3.1 solution containing 70 mM NaCl, 5 mM KCl, 4 mM $MgCl_2$, 10 mM $NaHCO_3$, 0.6 mM $CaCl_2$, 115 mM sucrose, 5 mM trehalose and 5 mM HEPES, pH 7.2.

Mass spectrometry. To enrich DNlg2 and its interacting proteins, DNlg2 tagged with EGFP was overexpressed using a ubiquitous driver (*da-GAL4*), and the protein complexes were extracted from lysates of *Drosophila* adult head tissue using the GFP-Trap Agarose (Chromotek). GFP overexpression served as the negative control. Afterwards, the fresh protein lysates were sent to Shanghai Applied Protein Technology Company for LC-MS. Trypsin was utilized as the incision enzyme. Proteins for *Drosophila melanogaster* from UniProt were used as a database and for analysis.

For the MS to detect the interacting proteins of the two terminals of DNlg2, the GST-tagged extracellular (M1-S965) and intracellular (A989-V1248) fragments of DNlg2 were expressed in the *E. Coli* and purified, respectively. These two fragments were then incubated with the fresh lysates of wildtype *Drosophila* adult head tissue, and further pulled down the protein complexes using the GST antibody and Pierce Protein A/G Agarose (Thermo Scientific).

Statistics and Reproducibility. All results are presented as mean ± SEM, and the data were analyzed using GraphPad Prism 9.0 software and Microsoft Excel. We assessed the significance between two groups using the two-tailed Student's t test, or the ordinary One-way ANOVA with multiple comparisons. A value of $P < 0.05$ was considered statistically significant. Asterisks indicate significant differences between genotypes: *$p < 0.05$, **$p < 0.01$, ***$p < 0.001$, ****$p < 0.0001$.

Reporting summary. Further information on research design is available in the Nature Portfolio Reporting Summary linked to this article.

Data availability

References

1. Südhof, T. C. Synaptotagmins: why so many? *J. Biol. Chem.* **277**, 7629–7632 (2002).
2. Sanes, J. R. & Lichtman, J. W. Development of the vertebrate neuromuscular junction. *Annu. Rev. Neurosci.* **22**, 389–442 (1999).
3. Vaughn, J. E. Fine structure of synaptogenesis in the vertebrate central nervous system. *Synapse* **3**, 255–285 (1989).
4. Jeong, S. Molecular mechanisms underlying motor axon guidance in drosophila. *Mol. Cells* **44**, 549–556 (2021).
5. Ali, H., Marth, L. & Krueger-Burg, D. Neuroligin-2 as a central organizer of inhibitory synapses in health and disease. *Sci Signal* **13**, eabd8379 (2020).
6. Banerjee, S., Venkatesan, A. & Bhat, M. A. Neurexin, neuroligin and wishful thinking coordinate synaptic cytoarchitecture and growth at neuromuscular junctions. *Mol. Cell Neurosci.* **78**, 9–24 (2017).
7. Banovic, D. et al. Drosophila neuroligin 1 promotes growth and postsynaptic differentiation at glutamatergic neuromuscular junctions. *Neuron* **66**, 724–738 (2010).
8. Bemben, M. A. et al. CaMKII phosphorylation of neuroligin-1 regulates excitatory synapses. *Nat. Neurosci.* **17**, 56–64 (2014).

9. Jedlicka, P. et al. Increased dentate gyrus excitability in neuroligin-2-deficient mice in vivo. *Cereb. Cortex* **21**, 357–367 (2011).
10. Jedlicka, P. et al. Neuroligin-1 regulates excitatory synaptic transmission, LTP and EPSP-spike coupling in the dentate gyrus in vivo. *Brain Struct. Funct.* **220**, 47–58 (2015).
11. Kim, J. V. et al. Neuroligin 2 regulates spinal GABAergic plasticity in hyperalgesic priming, a model of the transition from acute to chronic pain. *Pain* **157**, 1314–1324 (2016).
12. Medina, M. A. et al. Wnt/β-catenin signaling stimulates the expression and synaptic clustering of the autism-associated Neuroligin 3 gene. *Transl. Psychiatry* **8**, 45 (2018).
13. Song, J. Y., Ichtchenko, K., Südhof, T. C. & Brose, N. Neuroligin 1 is a postsynaptic cell-adhesion molecule of excitatory synapses. *Proc. Natl Acad. Sci. USA* **96**, 1100–1105 (1999).
14. Sun, M. et al. Neuroligin 2 is required for synapse development and function at the Drosophila neuromuscular junction. *J. Neurosci.* **31**, 687–699 (2011).
15. Tabuchi, K. et al. A neuroligin-3 mutation implicated in autism increases inhibitory synaptic transmission in mice. *Science* **318**, 71–76 (2007).
16. Uchigashima, M. et al. Specific Neuroligin3-αNeurexin1 signaling regulates GABAergic synaptic function in mouse hippocampus. *Elife* **9**, e59545 (2020).
17. Uchigashima, M., Ohtsuka, T., Kobayashi, K. & Watanabe, M. Dopamine synapse is a neuroligin-2-mediated contact between dopaminergic presynaptic and GABAergic postsynaptic structures. *Proc. Natl Acad. Sci. USA* **113**, 4206–4211 (2016).
18. Varoqueaux, F., Jamain, S. & Brose, N. Neuroligin 2 is exclusively localized to inhibitory synapses. *Eur. J. Cell Biol.* **83**, 449–456 (2004).
19. Xing, G. et al. Neurexin-Neuroligin 1 regulates synaptic morphology and functions via the WAVE regulatory complex in Drosophila neuromuscular junction. *Elife* **7**, e30457 (2018).
20. Yamagata, M., Sanes, J. R. & Weiner, J. A. Synaptic adhesion molecules. *Curr. Opin. Cell Biol.* **15**, 621–632 (2003).
21. Yoshida, T. et al. Canonical versus non-canonical transsynaptic signaling of neuroligin 3 tunes development of sociality in mice. *Nat. Commun.* **12**, 1848 (2021).
22. Zhang, X. et al. Neuroligin 4 regulates synaptic growth via the bone morphogenetic protein (BMP) signaling pathway at the Drosophila neuromuscular junction. *J. Biol. Chem.* **292**, 17991–18005 (2017).
23. Tian, Y., Zhang, Z. C. & Han, J. Drosophila studies on autism spectrum disorders. *Neurosci. Bull.* **33**, 737–746 (2017).
24. Chubykin, A. A. et al. Activity-dependent validation of excitatory versus inhibitory synapses by neuroligin-1 versus neuroligin-2. *Neuron* **54**, 919–931 (2007).
25. Poulopoulos, A. et al. Neuroligin 2 drives postsynaptic assembly at perisomatic inhibitory synapses through gephyrin and collybistin. *Neuron* **63**, 628–642 (2009).
26. Varoqueaux, F. et al. Neuroligins determine synapse maturation and function. *Neuron* **51**, 741–754 (2006).
27. Xing, G. et al. Drosophila neuroligin3 regulates neuromuscular junction development and synaptic differentiation. *J. Biol. Chem.* **289**, 31867–31877 (2014).
28. Chen, Y. C. et al. Drosophila neuroligin 2 is required presynaptically and postsynaptically for proper synaptic differentiation and synaptic transmission. *J. Neurosci.* **32**, 16018–16030 (2012).
29. Guangming, G., Junhua, G., Chenchen, Z., Yang, M. & Wei, X. Neurexin and neuroligins maintain the balance of ghost and satellite boutons at the drosophila neuromuscular junction. *Front Neuroanat.* **14**, 19 (2020).
30. Harris, K. P., Zhang, Y. V., Piccioli, Z. D., Perrimon, N. & Littleton, J. T. The postsynaptic t-SNARE Syntaxin 4 controls traffic of Neuroligin 1 and Synaptotagmin 4 to regulate retrograde signaling. *Elife* **5**, e13881 (2016).
31. Li, Y, et al. Drosophila neuroligin 4 regulates sleep through modulating GABA transmission. *J. Neurosci.* **33**, 15545–15554 (2013).
32. Mozer, B. A. & Sandstrom, D. J. Drosophila neuroligin 1 regulates synaptic growth and function in response to activity and phosphoinositide-3-kinase. *Mol. Cell Neurosci.* **51**, 89–100 (2012).
33. Corthals, K. et al. Neuroligins Nlg2 and Nlg4 affect social behavior in Drosophila melanogaster. *Front. Psychiatry* **8**, 113 (2017).
34. Cingolani, L. A. & Goda, Y. Actin in action: the interplay between the actin cytoskeleton and synaptic efficacy. *Nat. Rev. Neurosci.* **9**, 344–356 (2008).
35. Gautreau, A. M., Fregoso, F. E., Simanov, G. & Dominguez, R. Nucleation, stabilization, and disassembly of branched actin networks. *Trends Cell Biol.* **32**, 421–432 (2022).
36. Gentile, J. E., Carrizales, M. G. & Koleske, A. J. Control of synapse structure and function by actin and its regulators. *Cells* **11**, 603 (2022).
37. Konietzny, A., Bär, J. & Mikhaylova, M. Dendritic actin cytoskeleton: structure, functions, and regulations. *Front. Cell Neurosci.* **11**, 147 (2017).
38. Bernstein, B. W. & Bamburg, J. R. ADF/cofilin: a functional node in cell biology. *Trends Cell Biol.* **20**, 187–195 (2010).
39. Bamburg, J. R., McGough, A. & Ono, S. Putting a new twist on actin: ADF/cofilins modulate actin dynamics. *Trends Cell Biol.* **9**, 364–370 (1999).
40. Wang, W., Eddy, R. & Condeelis, J. The cofilin pathway in breast cancer invasion and metastasis. *Nat. Rev. Cancer* **7**, 429–440 (2007).
41. Rust, M. B. ADF/cofilin: a crucial regulator of synapse physiology and behavior. *Cell Mol. Life Sci.* **72**, 3521–3529 (2015).
42. Bamburg, J. R. & Bernstein, B. W. ADF/cofilin. *Curr. Biol.* **18**, R273–R275 (2008).
43. Ohashi, K. Roles of cofilin in development and its mechanisms of regulation. *Dev., growth Differ.* **57**, 275–290 (2015).
44. Bellenchi, G. C. et al. N-cofilin is associated with neuronal migration disorders and cell cycle control in the cerebral cortex. *Genes Dev.* **21**, 2347–2357 (2007).
45. Minamide, L. S., Striegl, A. M., Boyle, J. A., Meberg, P. J. & Bamburg, J. R. Neurodegenerative stimuli induce persistent ADF/cofilin-actin rods that disrupt distal neurite function. *Nat. cell Biol.* **2**, 628–636 (2000).
46. Bamburg, J. R. & Bloom, G. S. Cytoskeletal pathologies of Alzheimer disease. *Cell Motil. Cytoskelet.* **66**, 635–649 (2009).
47. Adams, D. R., Ron, D. & Kiely, P. A. RACK1, a multifaceted scaffolding protein: structure and function. *Cell Commun. Signal* **9**, 22 (2011).
48. Kadrmas, J. L., Smith, M. A., Pronovost, S. M. & Beckerle, M. C. Characterization of RACK1 function in Drosophila development. *Dev. Dyn.* **236**, 2207–2215 (2007).
49. Volta, V. et al. RACK1 depletion in a mouse model causes lethality, pigmentation deficits and reduction in protein synthesis efficiency. *Cell Mol. Life Sci.* **70**, 1439–1450 (2013).
50. Dopie, J. et al. Genome-wide RNAi screen for nuclear actin reveals a network of cofilin regulators. *J. Cell Sci.* **128**, 2388–2400 (2015).
51. Nakashima, A. et al. RACK1 functions in rice innate immunity by interacting with the Rac1 immune complex. *Plant Cell* **20**, 2265–2279 (2008).
52. Demarco, R. S. & Lundquist, E. A. RACK-1 acts with Rac GTPase signaling and UNC-115/abLIM in Caenorhabditis elegans axon pathfinding and cell migration. *PLoS Genet.* **6**, e1001215 (2010).
53. Cao, X. X. et al. RACK1 promotes breast carcinoma migration/metastasis via activation of the RhoA/Rho kinase pathway. *Breast Cancer Res. Treat.* **126**, 555–563 (2011).
54. Prokop, A. & Meinertzhagen, I. A. Development and structure of synaptic contacts in Drosophila. *Semin Cell Dev. Biol.* **17**, 20–30 (2006).
55. Chen, J. et al. Cofilin/ADF is required for cell motility during Drosophila ovary development and oogenesis. *Nat. Cell Biol.* **3**, 204–209 (2001).
56. Paavilainen, V. O., Bertling, E., Falck, S. & Lappalainen, P. Regulation of cytoskeletal dynamics by actin-monomer-binding proteins. *Trends Cell Biol.* **14**, 386–394 (2004).
57. Blunk, A. D. et al. Postsynaptic actin regulates active zone spacing and glutamate receptor apposition at the Drosophila neuromuscular junction. *Mol. Cell Neurosci.* **61**, 241–254 (2014).
58. Ng, J. & Luo, L. Rho GTPases regulate axon growth through convergent and divergent signaling pathways. *Neuron* **44**, 779–793 (2004).
59. Tu, R. et al. Proteolytic cleavage is required for functional neuroligin 2 maturation and trafficking in Drosophila. *J. Mol. Cell Biol.* **9**, 231–242 (2017).
60. Wagh, D. A. et al. Bruchpilot, a protein with homology to ELKS/CAST, is required for structural integrity and function of synaptic active zones in drosophila. *Neuron* **49**, 833–844 (2006).
61. Wu, J. et al. RACK1 promotes the proliferation, migration and invasion capacity of mouse hepatocellular carcinoma cell line in vitro probably by PI3K/Rac1 signaling pathway. *Biomed. Pharmacother.* **67**, 313–319 (2013).
62. Kershner, L. & Welshhans, K. RACK1 regulates neural development. *Neural Regen. Res.* **12**, 1036–1039 (2017).
63. Demarco, R. S. & Lundquist, E. A. "RACK"-ing up the effectors: Receptor for activated C kinase acts downstream of Rac GTPase signaling in growth cone outgrowth. *Small GTPases* **2**, 47–50 (2011).
64. Filho, E. G. F. et al. RACK1 plays a critical role in mast cell secretion and Ca2+ mobilization by modulating F-actin dynamics. *J Cell Sci* **134**, jcs252585 (2021).
65. Yang, H. et al. Opposite regulation of Wnt/beta-catenin and Shh signaling pathways by Rack1 controls mammalian cerebellar development. *Proc. Natl Acad. Sci. USA* **116**, 4661–4670 (2019).
66. Zhu, Q. et al. Rack1 is essential for corticogenesis by preventing p21-dependent senescence in neural stem cells. *Cell Rep.* **36**, 109639 (2021).
67. Machacek, M. et al. Coordination of Rho GTPase activities during cell protrusion. *Nature* **461**, 99–103 (2009).
68. Mackay, D. J., Nobes, C. D. & Hall, A. The Rho's progress: a potential role during neuritogenesis for the Rho family of GTPases. *Trends Neurosci.* **18**, 496–501 (1995).
69. Nobes, C. D. & Hall, A. Rho, rac, and cdc42 GTPases regulate the assembly of multimolecular focal complexes associated with actin stress fibers, lamellipodia, and filopodia. *Cell* **81**, 53–62 (1995).
70. Sit, S. T. & Manser, E. Rho GTPases and their role in organizing the actin cytoskeleton. *J. Cell Sci.* **124**, 679–683 (2011).

71. Agnew, B. J., Minamide, L. S. & Bamburg, J. R. Reactivation of phosphorylated actin depolymerizing factor and identification of the regulatory site. *J. Biol. Chem.* **270**, 17582–17587 (1995).

72. Li, Y. et al. Dual functions of Rack1 in regulating Hedgehog pathway. *Cell Death Differ.* **27**, 3082–3096 (2020).

73. Bischof, J., Maeda, R. K., Hediger, M., Karch, F. & Basler, K. An optimized transgenesis system for Drosophila using germ-line-specific phiC31 integrases. *Proc. Natl Acad. Sci. USA* **104**, 3312–3317 (2007).

74. Liu, A. et al. Neuroligin 1 regulates spines and synaptic plasticity via LIMK1/cofilin-mediated actin reorganization. *J. Cell Biol.* **212**, 449–463 (2016).

75. Ramachandran, P., Barria, R., Ashley, J. & Budnik, V. A critical step for postsynaptic F-actin organization: regulation of Baz/Par-3 localization by aPKC and PTEN. *Dev. Neurobiol.* **69**, 583–602 (2009).

76. Singh, S. K. et al. Astrocytes Assemble Thalamocortical Synapses by Bridging NRX1α and NL1 via Hevin. *Cell* **164**, 183–196 (2016).

77. Perez-Riverol, Y. et al. The PRIDE database resources in 2022: a hub for mass spectrometry-based proteomics evidences. *Nucleic Acids Res.* **50**, D543–d552 (2022).

Acknowledgements

Author contributions

M.L. and W.X. led the project. Y.S and M.L. designed the experiments and analyzed the data. Y.S. performed the experiments unless otherwise stated. J.G., and S.M. performed RACK1 and DNlg2 interaction assay in HEK293T. R.T., Y.Z., and G.X. performed mass spectrometry of DNlg2. M.S., M.R., and M.O. performed and analyzed RACK1 immunostaining assay. M.L., T.J. and Y.S. wrote and revised the manuscript.

Competing interests

The authors declare no competing interests.

Additional information

Supplementary information The online version contains supplementary material available at https://doi.org/10.1038/s42003-023-05428-3.

Correspondence and requests for materials should be addressed to Moyi Li or Wei Xie.

Peer review information *Communications Biology* thanks Christian Gonzalez-Billault and the other, anonymous, reviewer(s) for their contribution to the peer review of this work. Primary Handling Editors: Christian Wozny and Joao Valente.

Reprints and permission information is available at http://www.nature.com/reprints

Publisher's note Springer Nature remains neutral with regard to jurisdictional claims in published maps and institutional affiliations.